Nucleic Acid Amplification of Individual Molecules in a Microfluidic Device

ARTICLE *in* ANALYTICAL CHEMISTRY · JULY 2008

Impact Factor: 5.64 · DOI: 10.1021/ac800339w · Source: PubMed

Anal. Chem. **2008,** *80,* 4208–4213

Nucleic Acid Amplification of Individual Molecules in a Microfluidic Device

Roger Dettloff, Esther Yang, Aaron Rulison, Andrea Chow, and Javier Farinas*

Caliper Life Sciences, 605 Fairchild Drive, Mountain View, California 94024

A microfluidic device was developed that enabled rapid polymerase chain reaction (PCR) analysis of individual DNA molecules. The device combined a means for accessing samples serially from a microtiter plate, channels for assembling eight parallel PCR reactions, and integrated resistive heaters for rapid thermocycling (>5 °C/s heating, >7 °C/s cooling) of samples as they flowed continuously through PCR channels. Amplification was monitored by fluorescence detection of Taqman probes. The long, narrow channels (10 μm × 180 μm × 40 mm) allowed sufficient separation between neighboring DNA templates to enable amplification of discreet DNA molecules. The functionality of the device was demonstrated by reproducibly amplifying a 2D6.6 CYP450 template and distinguishing between wild-type and mutant sequences using Taqman probes. A comparison of the rate of individual amplification events to the expected Poisson distribution confirmed that the device could reliably analyze individual DNA molecules. This work establishes the feasibility of rapid, single-molecule interrogation of nucleic acids.

Clinical decisions often require analysis of heterogeneous nucleic acid mixtures. For example, during highly active antiretroviral therapy for patients infected with the human immunodeficiency virus, viral mutations develop which result in resistance to antiretroviral agents.[1] Minority viral populations play a key role in the development and progression of such resistance.[2] In such cases, it is important to be able to characterize the genotype of individual members of a viral population since analysis of the average genotype can miss important trends in developing drug resistance.[3] In another example, early detection of cancer often depends on the detection of rare mutant sequences in a background of wild-type sequences.[4] The similarity between the mutant and wild-type sequences can complicate the analysis of the rare mutants in a single reaction and thus require complex detection schemes.[5]

Methods such as "digital PCR",[6] whereby samples are serially diluted so that only single template molecules are present in individual wells subsequently analyzed by polymerase chain reaction (PCR), are capable of addressing both the genotyping of individual templates and the detection of rare sequences in a large background of wild-type sequence. The ability to analyze a heterogeneous mixture of nucleic acids by digital PCR is now being used for patient diagnosis.[7] However, digital PCR and similar limiting dilution schemes require a large number of PCR reactions resulting in high reagent cost and the need to assemble a large number of reaction wells.

Microfabricated devices have great potential to reduce the cost, complexity, and time required for PCR assays by reducing the volume of PCR reactions to tens of nanoliters,[8] integrating several assay steps into a single device, and rapidly thermocycling microchips with small dimensions.[9] The potential of microfluidic approaches to limiting dilution PCR has been demonstrated by performing a limiting dilution of templates that were separated spatially within a capillary.[10] The use of such an approach allowed discreet amplifications of templates to be detected; however, throughput was limited and the system was very labor intensive. Recently, a microfluidic digital PCR chip was reported.[11] The chip architecture allowed samples to be partitioned into 1176 reaction chambers. However, the number of reactions and reaction volumes were hardwired into the chip, and there was no flexibility in varying these parameters unless a different chip design was used.

In this report we describe a microfluidic system that was developed to overcome the high reagent cost and cumbersome reaction assembly requirements of plate-based limiting dilution PCR methods and the low throughput and manual handling of current microchip methods. Moreover, this device allows the number of reactions and the reaction volume to be flexibly

* To whom correspondence should be addressed. E-mail: farinas@pacbell.net. Fax: 650-623-0500.

(1) Erali, M.; Page, S.; Reimer, L. G.; Hillyard, D. R. *J. Clin. Microbiol.* **2001**, *39*, 2157–2165.
(2) Charpentier, C.; Dwyer, D. E.; Mammano, F.; Lecossier, D.; Clavel, F.; Hance, A. J. *J. Virol.* **2004**, *78*, 4234–4247.
(3) Palmer, S.; Kearney, M.; Malderelli, F.; Halvas, E. K.; Bixby, C. J.; Bazmi, H.; Rock, D.; Falloon, J.; Davey, R. T., Jr.; Dewar, R. L.; Metcalf, J. A.; Hammer, S.; Mellors, J. W.; Coffin, J. M. *J. Clin. Microbiol.* **2005**, *43*, 406–413.
(4) Mao, L.; Hruban, R. H.; Boyle, J. O.; Tockman, M.; Sidransky, D. *Cancer Res.* **1994**, *54*, 1634–1637.
(5) Sun, X.; Hung, K.; Wu, L.; Sidransky, D.; Guo, B. *Nat. Biotechnol.* **2002**, *19*, 186–189.
(6) Vogelstein, B.; Kinzler, K. *Proc. Natl. Acad. Sci. U.S.A.* **1999**, *96*, 9236–9241.
(7) Zhou, W.; Goodman, S. N.; Galizia, G.; Lieto, E.; Ferraraccio, F.; Pignatelli, C.; Purdie, C. A.; Piris, J.; Morris, R.; Harrison, D. J.; Paty, P. B.; Culliford, A.; Romans, K. E.; Montgomery, E. A.; Choti, M. A.; Kinzler, K. W.; Vogelstein, B. *Lancet* **2002**, *350*, 219–225.
(8) Wilding, P.; Shoffner, M. A.; Kricka, L. *J. Clin. Chem.* **1994**, *40*, 1815–1818.
(9) Woolley, A. T.; Hadley, D.; Landre, P.; deMello, A. J.; Mathies, R. A.; Northrup, M. A. *Anal. Chem.* **1996**, *68*, 4081–4086.
(10) Li, H.; Xue, G.; Yeung, E. S. *Anal. Chem.* **2001**, *73*, 1537–1543.
(11) Ottesen, E. A.; Hong, J. W.; Quake, S. R.; Leadbettter, J. R. *Science* **2006**, *314*, 1464–1467.

10.1021/ac800339w CCC: $40.75
Published on Web 05/07/2008

selected during run time instead of predetermined by the chip design. The microfluidic device allows for high-throughput, small volume interrogation of individual molecules by PCR. High throughput was obtained by using a continuous flow serial sampling system with eight parallel PCR reactors and rapid thermocycling capabilities. Precise temperature control was accomplished through nine resistive heating elements microfabricated adjacent to and sandwiching the eight channels through which PCR mixtures flow. The close proximity of the heaters to the reaction mixtures enabled rapid thermal cycling. Sample handling was minimized by introducing samples from a microtiter plate onto the microchip through an integrated capillary. Once inside the chip, samples were mixed with common and locus-specific reagents to assemble PCR reactions. The small channel dimensions used allowed reagent usage to be minimized and thermocycling to be conducted rapidly. This report describes the reproducibility of PCR in the device and the ability to analyze individual template molecules by spatially separating DNA along a long narrow channel.

EXPERIMENTAL SECTION

Microfluidic Chip: Design and Fabrication. Fabrication of the microfluidic chip was performed by photolithography and wet chemical etching using quartz substrate plates as previously described[12] with the following modifications. The resistive heaters were made on the bottom quartz plate from platinum traces formed using a standard photolithographic lift-off process. The metal traces lined up with etch relief features photolithographically defined on the top quartz plate that also contained the microfluidic channels. Silver epoxy adhesive was used as a conductive bridge between the metal traces and the instrument electrodes. The channels and electrodes were at the midpoint of the 1.45 mm thick chips. After the chip was bonded, a silica capillary (320 μm o.d., 30 μm i.d., 25 mm length) was inserted into a hole perpendicular to the bottom plate and glued in place[13] such that the lumen of the capillary was fluidically connected to the microchannel network of the planar device. The plastic caddy glued to the top surface of the chip contained wells for common PCR reagent mix, locus-specific reagents, waste wells, and electrical contact to the platinum heater traces. The reagent wells, which were 5 mm high and had a diameter of 4 mm, were filled with ~10 μL of reagents.

As shown in Figure 1A, a channel connected the capillary to the common reagent well and then split into eight parallel channels. Each of these eight channels was connected to an independent locus-specific reagent well and then was routed between two of the nine resistive heater elements. The common reagent wells held the dNTPs and Taq polymerase while the locus-specific wells contained the probes and primers. Each channel in the thermocycling region was 10 μm × 180 μm × 40 mm. After the thermocycling region, the channels narrowed to 45 μm and were grouped into a multichannel detection region and then terminated in eight waste wells. With the buffers used in this study, 58% of the flow came from the capillary, 14% from the

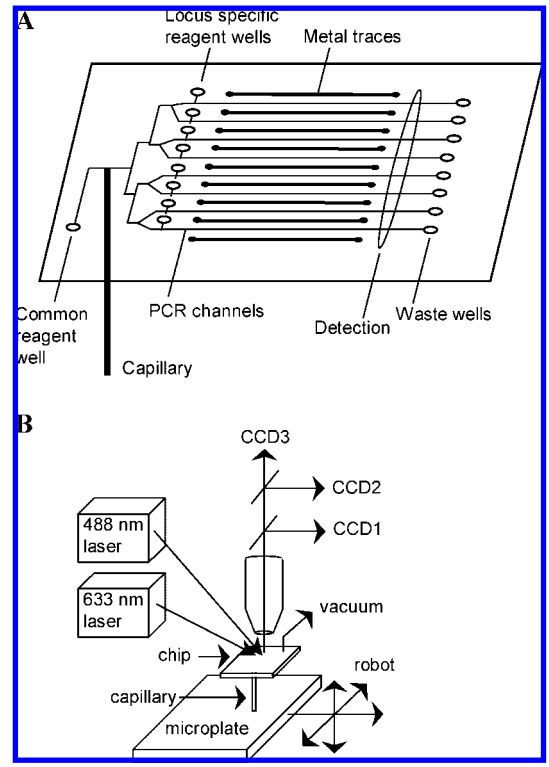

Figure 1. (A) Schematic of the channels in the PCR chip. The metal traces were 1 mm apart with each channel at the midpoint between adjacent metal traces. (B) Schematic of instrumentation.

common reagent well, and 28% from the locus-specific well. The channel hydrodynamic resistances were designed so that a vacuum of −2 psi applied to the waste well resulted in a flow rate of 0.0972 nL/s per channel and a transit time through the thermocycling region of 711 s. An additional 178 s were required for the amplicons to reach the detection region.

In the design of this chip, adequate mixing by Brownian diffusion after each stage of reagent dispensing was a criterion. For instance, after addition of the common reagents, the channel width and length were selected to ensure that the slowest diffusing species, namely, the Taq polymerase, had sufficient time to diffuse across the width of the channel before the subsequent flow splitting junction under the nominal flow conditions of −2 psi.

PCR Amplification. PCR was performed on synthetic CYP2D6.6 wild-type and mutant templates using a PCR buffer containing 50 mM Tris−HCl pH 8.3, 50 mM KCl, 10 μM EDTA, 1 M Betaine, 0.04% Tween-20, 2% DMSO, 0.2 U/μL AmpliTaq, 4.25% glycerol, 200 μM dATP, dGTP, dCTP, dTTP, 4 mM $MgCl_2$, 300 nM mutant probe, 300 nM wild-type probe, 1 μM forward and 1μM reverse primers. Forward primer (5′ TGG GCC TGG GCA AGA AG 3′), reverse primer (5′ GCG AAG GCG GCA CAA A 3′), wild-type probe (5′ VIC−CGG TCA CCC ACT GCT CCA GC−TAMRA 3′), and mutant probe (5′ 6FAM−CGG TCA CCC CTG CTC CAG C−TAMRA 3′) were purchased from Applied Biosystems (Foster City, CA). PCR amplification was carried out with 30−40 cycles at 87 °C for 3 s, 58 °C for 11 s, and 70 °C for 3 s. The number of cycles could be varied by changing the residence time in the thermocycling region by varying the vacuum pressure at the waste wells. Typically a pressure of −2 psi was used with the 17 s cycle to yield 40 PCR cycles. Calibration of

(12) Cohen, C. B.; Chin-Dixon, E.; Jeong, S.; Nikiforov, T. T. *Anal. Biochem.* **1999**, *273*, 89–97.
(13) Farinas, J.; Chow, A. W.; Wada, H. G. *Anal. Biochem.* **2001**, *295*, 138–142.

channel temperature was performed by monitoring the fluorescence of a DNA melting probe (5′ TET−GCG GCC ACA CAC T 3′ and 5′ AGT GTG TGG CCG C−Dabcyl 3′) having a melting temperature of 68.5 °C.

Instrumentation. The microfluidic chip was placed in a custom instrument shown schematically in Figure 1B. The metal traces inside the chip were heated by applying time varying input power independently to each metal trace. Chilled recirculating water (22 ± 0.1 °C) was flowed underneath the chip to provide a well-defined heat transfer interface that allowed for rapid temperature transitions and predictable and stable steady-state temperatures across all eight PCR channels. The electrical resistance and temperature coefficient of electrical resistance of each metal trace was determined through calibration against standard thermocouples. The electrical resistance was then monitored as a measure of metal trace temperature. A thermal model was developed to determine the set of nine metal trace temperatures that would result in the desired microfluidic channel temperature, which was set the same for all eight microfluidic channels but varied in time. A thermocouple in contact with the top surface of the chip was used to monitor the temperature transitions. An *XYZ* robot was used to position a microtiter plate containing samples underneath the chip to allow the capillary to withdraw materials from individual wells. The capillary was used to sample wells of a 384-well PCR plate (ABI no. 4309849). The wells were conical 3 mm × 10 mm and filled with 40 μL of sample. The plate was kept at 20 °C and 50% RH and covered when not being accessed in order to limit evaporation from the wells. Vacuum was applied through a manifold to all eight waste wells to draw fluid through the chip. After accessing a sample for a desired period, typically ranging from 50 to 1000 s, the capillary was washed in a trough containing recirculating buffer. Buffer was sipped onto the chip for 200−500 s to allow for adequate washing and to introduce a buffer spacer between samples. For optical detection, a 488 nm optically pumped solid-state laser and the 633 nm line of a HeNe laser were spread across the eight channels in the detection zone. A 10× objective was used to capture the emitted fluorescence. Fluorescence was passed through a series of dichroic mirrors and band-pass filters (centered at 515, 550, and 685 nm) before being collected by three CCD cameras. Custom software converted the spatial CCD signals into intensity data for each of the eight channels. Fluorescence data was acquired at 1 Hz.

RESULTS AND DISCUSSION

The ability to rapidly thermocycle the chip was demonstrated by measuring the temperature of the top chip surface while cycling the channel temperature from 60 to 72 to 90 °C for 9 s per temperature. Metal trace, top chip surface, and recirculating water temperatures are shown in Figure 2A. The channel temperatures were intermediate between the top and bottom chip surface temperatures. The metal trace temperatures rapidly reached steady state (>20 °C/s) while the top chip surface temperature showed that heating (>5 °C/s) and cooling rates (>7 °C/s) were lower than the trace rates. The temperature transition rates for the channels are expected to be between the transition rates for the traces and the top chip surface. To verify that the correct channel temperatures could

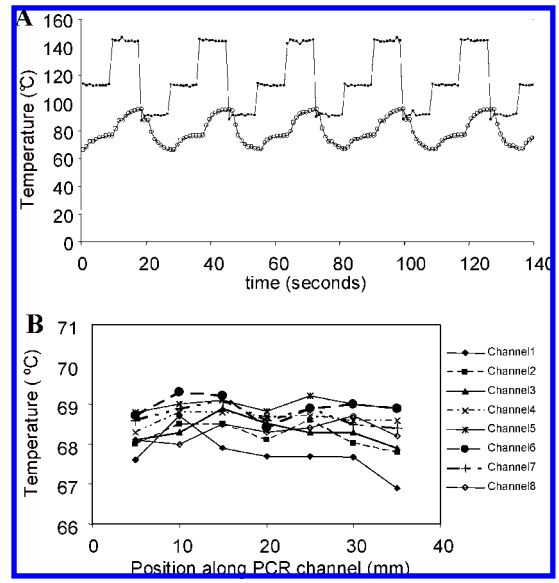

Figure 2. Embedded heaters enabled rapid and accurate thermocycling. (A) Temperature profile of top chip surface (circles), heater trace (filled squares), and bottom chip surface (dashed line) using channel temperature set points of 60, 72, and 90 °C each for 9 s. (B) Temperature uniformity across the chip determined by DNA melting probe when the channel temperature set point was 68.5 °C.

be attained, the temperature in each channel was mapped by using optical DNA melt probes and compared to the desired set point. As shown in Figure 2B, when the desired channel temperature was 68.5 °C deviations from the set point were typically less than 1 °C throughout the channels.

To demonstrate that efficient and reliable PCR amplification could be conducted, a series of samples was sipped onto the chip and amplification of the CYP2D6.6 alleles was monitored. As seen in Figure 3A, high concentrations (30 copies/nL) of wild-type, mutant, or a 1:1 mixture of wild-type and mutant template were readily distinguished based on the measured fluorescence of the Taqman probes at 515 and 550 nm. Amplification of wild-type templates yielded higher 550 nm fluorescence, whereas mutant templates yielded higher 515 nm fluorescence. Amplification was quantified by measuring the height of the fluorescence signals. At the high template concentrations, amplification from closely packed template molecules merged to give a plateau of amplified product. For all experiments, DNase (1.8 U/mL) was sipped periodically between samples to ensure that the no-template control (NTC) showed no amplification due to carryover from previous samples.

The reproducibility of the amplification was demonstrated by measuring the amplification of five samples across two instruments, eight chips, and eight channels per chip (320 total replicates). As seen in Figure 3B, there was excellent discrimination among the wild-type, mutant, 1:1 mixture of wild-type and mutant, and the no-template control. Reproducibility was quantified by measuring the average and standard deviation of the polar coordinate magnitude ($r = (F_{515nm}{}^2 + F_{550nm}{}^2)^{1/2}$) and angle ($\theta = \tan^{-1}(F_{550nm}/F_{515nm})$) for each sample type. Table 1 summarizes the averages, standard deviations, and signal-to-noise ratios for the parameters. The signal-to-noise ratio of the magnitude was a measure of the ability to determine whether amplification had

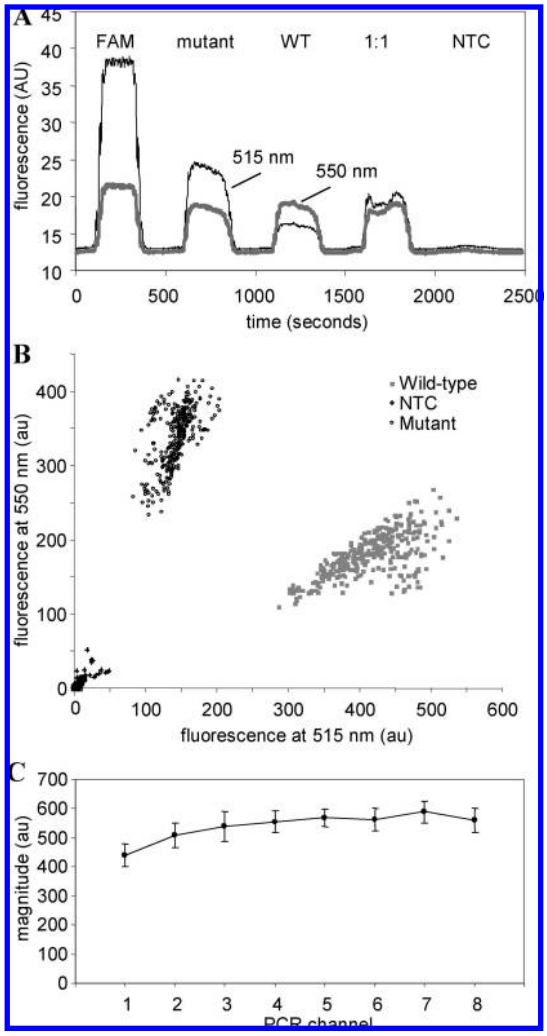

Figure 3. PCR amplification was robust. (A) Raw data shows amplification signal for samples introduced onto the chip. FAM (100 nM) was used as an optical reference. Mutant and wild-type samples were at a total template concentration of 30 copies/nL in the PCR channels. (B) Replicate ($n = 320$) fluorescence signals for wild-type, mutant, and no-template control (NTC) samples showed clear separation among sample types. (C) Signal magnitude and the variability of the magnitude were fairly uniform across all eight channels (mean ± SD).

Table 1. Signal-to-Noise Ratio and Variability of the Genotyping Assay[a]

	NTC	wild-type	mutant
magnitude (au)	9.6 ± 8.6	367 ± 41	452 ± 56
angle (radians)	0.78 ± 0.17	1.17 ± 0.043	0.40 ± 0.042
$S/N_{magnitude}$		7.2	6.8
S/N_{angle}		9.0	9.0

[a] Values are reported as mean ± standard deviation with 320 replicates. $S/N_{magnitude} = |magnitude_{sample} - magnitude_{NTC}|/(|SD_{sample} + SD_{NTC})$; $S/N_{angle} = |angle_{WT} - angle_{Mut}|/(|SD_{WT} + SD_{Mut})$.

taken place, whereas the signal-to-noise ratio of the angle was a measure of the ability to distinguish between the two types of alleles. As shown in Table 1, the signal-to-noise ratios for both the magnitude and angles were >6, whereas the CVs for each sample measurement were <13% indicating a robust assay capable of distinguishing whether a sample was amplified and the identity

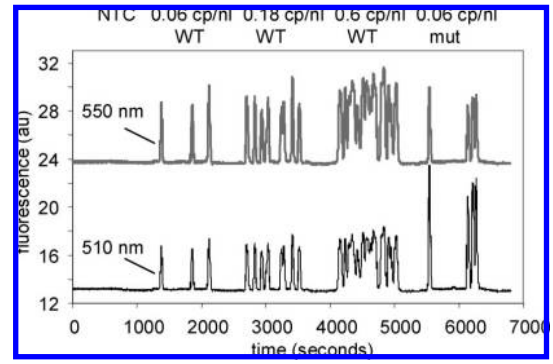

Figure 4. Single-molecule PCR amplification. Fluorescence signals for the indicated template concentrations of wild-type and mutant templates showed the ability to count individual DNA molecules and to distinguish between template types.

of the amplified product. As shown in Figure 3C, amplification was fairly uniform across all eight channels. The slight differences in signal in the outer channels were most likely due to minor differences in temperatures among the channels (compare to temperatures in Figure 2B). Further refinement of the power applied to the outer metal traces should correct the problem. Some of the remaining variability was due to channel-to-channel differences in the efficiency of fluorescence excitation across the channels (data not shown).

The long narrow PCR channels allowed dilute template molecules to be spaced far enough apart that the amplification products of one template did not mix with the amplification products of its nearest neighbor. This effect was demonstrated in Figure 4 which shows the fluorescence during times when an NTC, a wild-type template at 0.06, 0.18, or 0.6 copies/nL, and a mutant template at 0.06 copies/nL were analyzed on the chip. At the low concentration, discreet events were seen, which became more frequent as the concentration increased, and eventually the individual events merged to give the beginning of a plateau of amplified products. Comparison of Figure 4 and Figure 3A shows that the peak values of the fluorescence signals were about the same when the initial average template concentrations varied by a factor of 50. This was due to the fact that no matter what the initial average template concentration, the PCR reaction locally reached a plateau phase where the fluorescence intensity was not greatly dependent on the initial local template concentration. Under these conditions, individual templates were expected to be detected at rates of 5, 15, and 50 events per 1000 s, respectively. As expected, discreet amplification events were seen with wild-type samples showing larger 550 nm fluorescence signals and mutant samples showing larger 515 nm fluorescence signals. Given the observed time for the amplification peak to pass the detector (~30 s peak width at half-height) and flow velocity of 0.22 mm/s, the amplification events are approximately 6.6 mm wide by the time that they reached the detector.

The width of the events is governed by the Taylor−Aris dispersion coefficients[14,15] of amplicons in the PCR and detection channels:[16]

$$K = D + fv^2h^2/(210D)$$

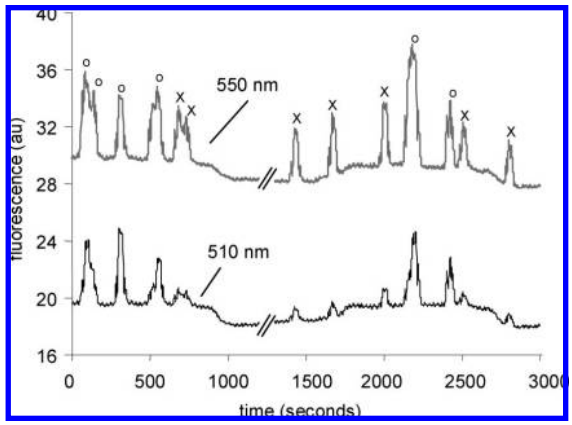

Figure 5. Distinguishing individual templates in heterogeneous samples. Fluorescence signals for a 1:1 mixture of wild-type and mutant templates at a total concentration of 0.06 copies/nL were used to discriminate between wild-type (○) and mutant (×) template molecules.

where K is the Taylor−Aris dispersion coefficient, D is the diffusion coefficient of the amplicon, $v$is the flow velocity, f is a factor which depends on the channel cross section, and h is the channel height. Under the flow conditions used in this study, with the amplicon diffusion coefficient estimated to be 5×10^{-7} cm^2/s, the Taylor−Aris dispersion coefficients in the PCR and detection channels are 3.0×10^{-6} and 2.9×10^{-5} cm^2/s, respectively. Applying the Einstein equation for diffusion, variance (σ^2) $\sim 2Kt$, and the measured travel times (t) in the thermocycling region and in the detection region, the estimated final peak width of 6.9 mm for single-molecule amplified event agrees well with the observed value.

To confirm that the observed signals were due to amplification of discreet templates, mutant templates at 0, 0.01, or 0.1 copies/nL were sampled for 50 s each. Given the flow rates and concentrations, calculations based on the Poisson distribution predicted that sample plugs introduced onto the chip would contain templates 0%, 2.8%, and 24.6% of the times, respectively. Sampling 1362 wells of each concentration resulted in 0.1%, 2.9%, and 21.5% of samples with amplification of mutant template. The excellent agreement between the expectations based on the Poisson distribution of individual molecules and the observed amplification confirms that individual molecules can be interrogated using microfluidic PCR.

The utility of the device was demonstrated by genotyping individual molecules from a sample. As shown in the sample data in Figure 5, when a sample consisting of a 1:1 mixture of wild-type and mutant templates was analyzed, discreet amplification events corresponding to either wild-type or mutant sequences were observed. For all of the measured events on two separate runs, 48.4% of the events were characterized as wild type, very close to the expected 50%.

As seen in Figure 5, the fluorescence peaks have periodic "spikes" superimposed on the signal. These spikes are in sync with the heater cycle timing, and they disappear when the thermocycling is turned off (data not shown). Interestingly, the origin of the spikes comes from the differential coefficients of thermal expansion between the chip and the reaction mixture flowing through the channel. At the transition from high to low temperature, the fluid contained in the channel contracts a little more than the channel, resulting in a momentary change in the flow direction. At the detection point, a spike is seen when the peak gets pulled back under the detector during the transient flow. Because temperature increases occur in two steps, spikes were not noticeable when the temperature transitioned from low to high.

One potential concern about the thermocycling-induced spikes in velocity is that it may substantially increase the dispersion of the peak, because it has been known that pulsating shear flow tends to increase dispersivity in Taylor−Aris flow.[17] On the other hand, the experimentally measured peak widths were in good agreement with predicted values as discussed earlier, so there appears to be minimal additional dispersivity resulting from the fluid expansion−contraction effects. To understand this phenomenon better, we conducted a particle dynamics simulation to model the peak broadening with and without velocity spikes. Over 1000 particles seeded in a narrow band along with an appropriate diffusion coefficient (for dye and for amplicon) were tracked in the simulation, with "bounce-back" reflection from the walls of the channel. The three-dimensional kinematics under pressure-driven flow in a rectangular channel was used as the average velocity at any one time step, and the temporal velocity variance due to thermal expansion and contraction was superimposed on top of the average mimicking experimental thermocycling time intervals. The simulation confirmed that there was no observable increase in variance in dye or amplication peaks, mainly due to the fact that the duration of the velocity disturbance due to thermal effects was too short.

As shown in Figure 4, at a concentration of 0.18 cp/nL the microfluidic device allows processing of ∼8 discreet, well-resolved templates per channel per 1000 s. With the current eight channel device ∼96 templates could be analyzed in 25 min using ∼1 μL of PCR reaction volume. This sample throughput compares favorably with the results from previous limiting dilution methods. Digital PCR[6] required two 96-well plates to analyze 96 templates in 2 h using ∼1.4 mL of PCR reaction volume. Detection of individual templates using capillary PCR[10] allowed 10 templates to be analyzed in 0.35 μL in 100 min. Resolution between the templates was poor. The current microfluidic device could be improved to yield a higher template throughput by reducing dispersion of amplification thus allowing more templates to be analyzed per unit time or by increasing the number of parallel PCR reaction channels. Reducing the dispersion coefficient by reducing the channel height from 10 to 5 μm would allow twice as many amplicons to be packed in the same space. In the current design, transport through the narrow detection channel accounts for greater than half of the peak dispersion. By moving the optical detection region closer to the end of the PCR channels and maintaining the width of the PCR channel through the detection zone the dispersion could be reduced by a factor of 3. Together these changes would result in an amplication event width of ∼1 mm and thus a 6-fold increase in throughput. With the use of the current device footprint, 2−4 times as many channels could

(14) Taylor, G. *Proc. R. Soc. London, Ser. A* **1953**, *219*, 186–203.
(15) Aris, R. *Proc. R. Soc. London, Ser. A* **1956**, *235*, 67–77.
(16) Dutta, D.; Leighton, D. T., Jr *Anal. Chem.* **2001**, *73*, 504–513.
(17) Aris, R. *Proc. R. Soc. London, Ser. A* **1960**, *259*, 370–376.

be incorporated into the device. Combined, these changes would allow ~2300 templates to be processed in 25 min.

CONCLUSIONS

The results presented here demonstrate the robustness and utility of a microfluidic single-molecule PCR amplification device. Although overall reproducibility was good, further refinement of the heating protocol should eliminate the small channel-to-channel differences in amplification. The current device allows a large number of individual templates to be analyzed while minimizing the amount of required reagents and the amount of liquid handling required to assemble PCR reactions. The current device relies on fluorescence emission wavelength as a means of distinguishing amplicons. Future instruments could be designed that would integrate either thermal melt analysis or electrophoretic separation in order to enhance the ability to distinguish amplicons.

ACKNOWLEDGMENT

We thank Cheryl Cathey and Wally Parce for technical discussions, the Caliper Hardware and Software groups for making the instrument, and Mac McReynolds, Knute Stevenson, and Khushroo Ghandi for fabricating the microfluidic chips. We also thank Deborah Boles and Ivor Knight of Canon U.S. Life Sciences for support for this project.

Received for review February 18, 2008. Accepted March 31, 2008.

AC800339W